Dalton Transactions

ROYAL SOCIETY OF CHEMISTRY

PAPER

View Article Online
View Journal | View Issue

Cite this: *Dalton Trans.*, 2025, **54**, 4566

An insight into the route from CO_2 fixation to CO_3^{2-}-bridged dinuclear lanthanide(III) complexes featuring inner coordination post-synthetic modification†

Vaibhav Singh, Vajeeha Urunikulavan and Arun Kumar Bar *

Received 31st October 2024,
Accepted 3rd February 2025

DOI: 10.1039/d4dt03050h

rsc.li/dalton

An insight into the route from the fixation of CO_2 gas into CO_3^{2-} and the concomitant formation of a novel series of carbonato-bridged dinuclear lanthanide(III) complexes is presented. Efficient and quantitative conversion of CO_2 gas into CO_3^{2-} is confirmed by deliberately employing CO_2 gas as a reagent. The feature of inner coordination post-synthetic modification is demonstrated *via* ligand substitution at the terminally axial coordination sites of the dinuclear motifs. Spectroscopic and X-ray crystallographic techniques were employed for probing the reactions and structural elucidation of the products.

Introduction

Excessive amount of greenhouse gas CO_2 in the atmosphere is a serious concern.[1] An enormous amount of effort is being directed to mitigate it.[2] Various chemical routes are being employed to capture atmospheric CO_2 and convert it into value-added products.[3] Notably, lanthanide (Ln) elements possess immense potential in this regard, primarily due to their high affinity towards oxygenated species.[4] It has been observed on numerous occasions that Ln(III) complexes capture atmospheric CO_2 to result in hierarchical complexes incorporating versatile binding modes of inorganic carbonates.[3f,g] The general procedure for the formation of such carbonato complexes is as follows. Trivalent lanthanide salts were treated with various organic ligands in the presence of a base in alcoholic media. The reaction mixtures were kept aside under aerobic conditions for crystallization by slow evaporation of the reaction media. Such a sequence of processes is found to result in the crystallization of versatile inorganic carbonato metal clusters.[5] However, there is also precedence to obtain carbonato Ln(III) complexes by employing CO_2 gas as a reaction ingredient.[5s] Surprisingly, to the best of our knowledge, the investigation is extensively limited to the characterization of the isolated end-products in their solid states. Little is known about the reaction media during the course of the reactions pertaining to the carbonato Ln complexes. Thus, we intended to investigate the progress of the reactions *en route* to the formation of the carbonato Ln complexes. Moreover, post-synthetic modification in the inner coordination environments of the Ln-based complexes is extremely challenging.[6] Therefore, we also intended to explore if the carbonato lanthanide complexes could be endowed with the feature of inner coordination post-synthetic modification. Herein we report a simplistic synthetic strategy for efficient conversion of CO_2 gas into CO_3^{2-} and the concomitant formation of a novel series of carbonato-bridged dinuclear lanthanide(III) complexes (Scheme 1). The post-synthetic modification is demonstrated by the substitution reactions at the terminally axial coordination sites of the dinuclear motifs (Scheme 1). The progress of the reactions has been thoroughly investigated by spectroscopic and X-ray crystallographic techniques to decipher the associated products comprehensively.

Y(III) was chosen in the current studies for convenient NMR spectroscopic analyses considering its diamagnetic nature. The chemical reactivity of Ln ions is mostly governed by their ionic size and Lewis acidity.[7] Thus, Er(III) was included in the current studies in order to verify the generality of lanthanides as Er(III) has a similar ionic radius and Lewis acidity to Y(III).[7] The pentadentate ligand, H_2L, is employed herein since such a ligand is well known to endow Ln(III) complexes with structural rigidity over a wide range of reaction conditions.[8] The chemical shift corresponding to the CH_3 moieties of H_2L is found to be considerably sensitive to the coordination environment around the Ln centers. Moreover, it is well separated from the rest of the signals of H_2L (Fig. 1). Consequently, one could obtain information about the products in the reaction solutions by monitoring their ^1H NMR spectra.

Department of Chemistry, Indian Institute of Science Education and Research Tirupati, Tirupati – 517619, Andhra Pradesh, India.
E-mail: a.bar@iisertirupati.ac.in

† Electronic supplementary information (ESI) available: Experimental procedure along with the supplementary data and their analysis plots related to UV-vis, PL, IR, and NMR spectroscopy, single crystal and powder X-ray crystallography, and DFT computations. CCDC 2378627–2378634. For ESI and crystallographic data in CIF or other electronic format see DOI: https://doi.org/10.1039/d4dt03050h

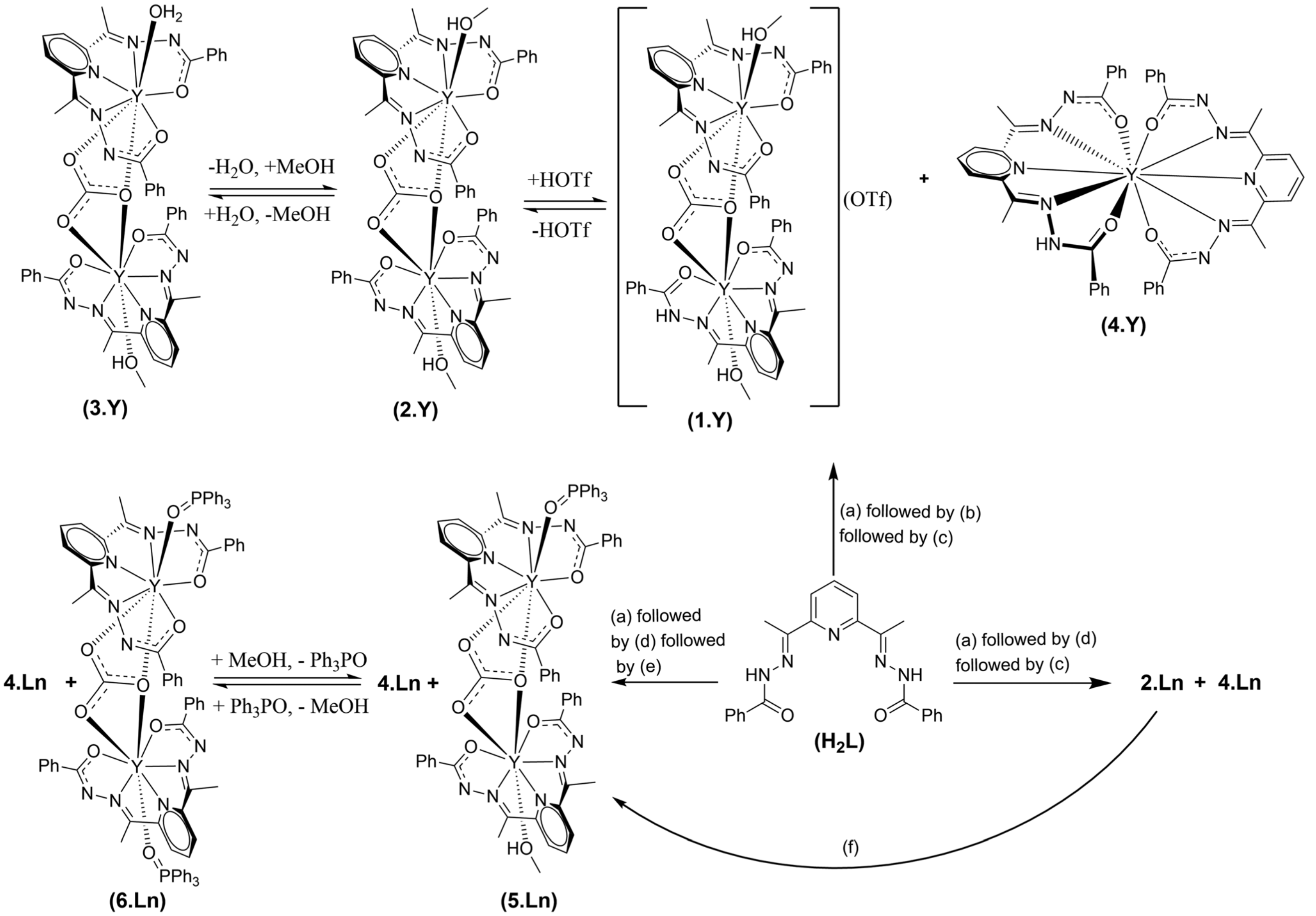

Scheme 1 Schematic representation for the conversion of CO_2 gas into CO_3^{2-} as the bridging ligand and the formation of dinuclear complexes **1·Ln–3·Ln**, **5·Ln**, and **6·Ln** and the formation of the mononuclear decacoordinate complex **4·Ln**. The generic reaction conditions are (a) H_2L + $Y(OTf)_3\cdot 6H_2O$ (1 : 1 mol/mol), aqueous methanol, stirring for 5 min, room temperature; (b) Et_3N (2 equiv., with respect to H_2L, mol/mol), *in situ*, stirring for 5 min, room temperature; (c) purging of CO_2 gas, stirring for 5–10 min, room temperature; (d) Et_3N (3 equiv., with respect to H_2L, mol/mol), *in situ*, stirring for 5 min, room temperature; (e) Ph_3PO, *in situ*, room temperature; and (f) Ph_3PO, into the methanolic solutions of the isolated **2·Ln**, room temperature. Ln = Y for **1·Ln** and **3·Ln**. Ln = Y and Er for **2·Ln** and **4·Ln–6·Ln**.

Experimental section

Materials and methods

All the reagents and solvents used for the syntheses were used as received from commercial suppliers. The Schiff base ligand H_2L was synthesized following the reported procedure.[9] Triphenylphosphine oxide (Ph_3PO) was synthesized starting from triphenylphosphine following the reported procedure.[10] Synthetic manipulations and sample processing for all the characterization studies in solutions were carried out under anaerobic conditions for all the complexes unless otherwise mentioned. All the spectroscopic studies were carried out under ambient conditions. UV-Vis and fluorescence spectral studies were carried out on μ(M) methanol solutions or solid samples using a CARY 3500 Compact UV-Vis spectrophotometer and Jasco FP-8500 spectrofluorometer, respectively. The ^1H and ^{31}P NMR spectral studies were carried out for the Y analogues of the complexes in deuterated methanol (CD_3OD) using a Bruker Ascend 400 FT-NMR Spectrometer. Fourier transform infrared (FT-IR) spectroscopic studies were performed on the thin layers of neat samples with a Bruker-Alpha Eco-ATR FT-IR spectrometer.

Photoluminescence studies

Photoluminescence excitation spectra were recorded with excitation wavelengths ranging from 200 to 700 nm for methanolic solutions and from 250 to 500 nm for solid samples. Emission wavelengths ranged from 210 to 800 nm (1 nm intervals) for methanolic solutions and from 260 to 800 nm (1 nm intervals) for solid samples, using excitation and emission bandwidths of 2.5 nm and a scanning speed of 1000 nm min^{-1}. Both the solid-state and solution fluorescence emission spectra were recorded at excitation wavelengths corresponding to λ_{max} values obtained from UV-Vis studies, with 2.5 nm bandwidths, a data interval of 0.1 nm, and a scanning speed of 500 nm min^{-1} under high-sensitivity conditions. Additionally, emission spectra of **2·Y** (λ_{ex} = 392 nm, 340 nm), **5·Y** (λ_{ex} = 392 nm, 342 nm), **2·Er** (λ_{ex} = 392 nm, 341 nm), and **5·Er** (λ_{ex} = 392 nm,

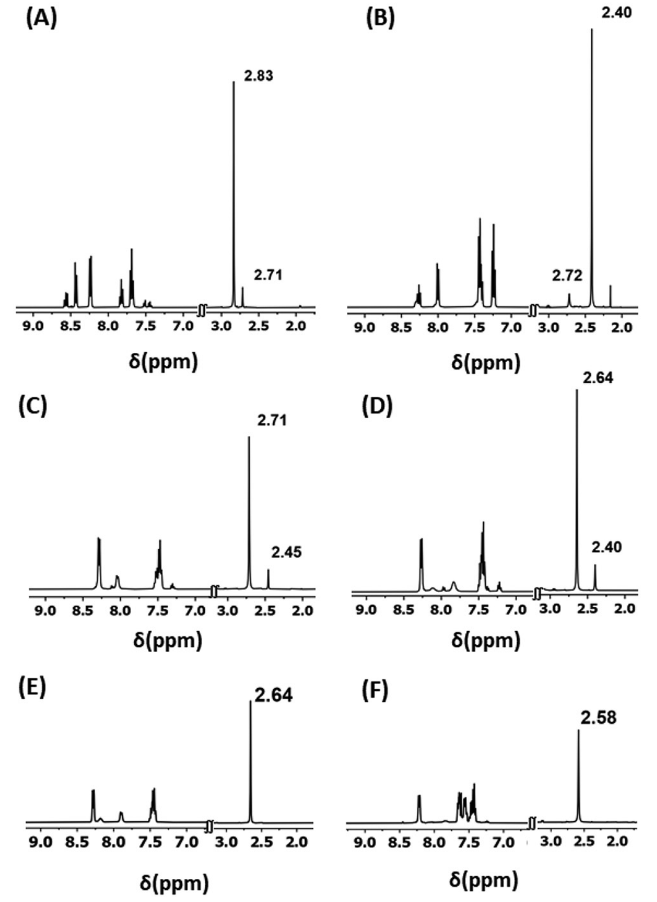

Fig. 1 The partial ^{1}H NMR spectra of (A) the reaction mixture of (a) as described in Scheme 1, (B) the reaction mixture of (a) followed by (b), (C) the reaction mixture of (a) followed by (b) followed by (c), (D) the reaction mixture of (a) followed by (d) followed by (c), (E) isolated **2·Y**, and (F) isolated **5·Y**. The chemical shifts corresponding to the $-CH_3$ moieties are labelled. The corresponding full spectral ranges are provided in Fig. S1–S9 in the ESI.† All the NMR spectral studies were carried out in CD_3OD solvent at room temperature.

342 nm) in their μM methanolic solutions were recorded with excitation and emission bandwidths of 10 nm and 5 nm, respectively, and a scanning speed of 500 nm min^{-1} under high-sensitivity conditions. These spectra are shown as insets in Fig. 5.

X-ray crystallographic studies

Suitable single crystals for X-ray diffraction were coated with paratone oil and mounted onto a goniometer. The X-ray crystallographic data were obtained using a Bruker (D8 Advance, Da Vinci) diffractometer using a Mo-Kα radiation source and equipped with an Oxford Cryo-system. The structures have been solved by direct methods using SIR92 or Superflip and refined by means of least-square procedures on F using the PC version of the program Olex2. The scattering factors for all the atoms were used as listed in the International Tables for X-ray Crystallography.[11] Absorption correction was performed using a multi-scan procedure. The H atoms were repositioned geometrically. The H atoms were initially refined with soft restraints on the bond lengths and angles to regularize their geometry and U_{iso}(H) (in the range 1.2–1.5 times U_{eq} of the parent atom), after which the positions were refined with riding constraints. All non-hydrogen atoms were refined anisotropically. Crystallographic data and refinement parameters for the single-crystal X-ray data analyses for all the complexes are summarized in Tables S5 and S6.† The selected bond parameters are provided in Table S7.† CIF files have been deposited at the CCDC with references 2378627–2378634 for the complexes **1·Y**, **2·Y**, **3·Y**, **4·Y**, **5·Y**, **6·Y**, **2·Er** and **5·Er**. The solid-state phase purity of the isolated polycrystalline solid samples of the complexes was confirmed by powder X-ray diffraction (PXRD) using a Rigaku (SmartLab) diffractometer with a Cu-Kα radiation source, $\lambda = 1.5406$ Å. The PXRD studies were carried out with 2θ ranging from 5 to 50° with a step size of 0.01.

Gas-phase IR studies

In order to investigate the efficiency of the capture and conversion of CO_2 gas, gas-phase FT-IR spectroscopic studies in conjunction with gasometer spectroscopic analyses were carried out on the headspace of the reaction mixture of the Y analogue. The reaction with three equivalent Et_3N was performed in a home-made *H*-type Schlenk tube under the same reaction conditions as above (see the synthetic details). At the stage of the reaction after the addition of a base ((a) followed by (d); Scheme 1), the Schlenk tube was charged with one equivalent CO_2 gas using a home-made manometer. The equivalency of CO_2 gas was calculated based on the yield of **2·Y** as observed in the aforementioned NMR studies on the reaction mixture, assuming the ideal-gas behaviour of CO_2 gas. The analyses were carried out on the headspace of the reaction Schlenk tube.

Determination of the solubility product

A sample of 0.7 mg of **2·Y** was dissolved in 50 mL methanol using a volumetric flask. The UV-vis absorbance ($A_1 = 0.7416$ a.u.) was measured at $\lambda_{\max} = 340$ at STP. A saturated solution of **2·Y** was prepared in methanol as a stock solution at STP. An aliquot of 200 μL stock solution was diluted to a 2 mL solution at STP. The UV-vis absorbance ($A_2 = 0.3376$ a.u.) was measured for the diluted solution at $\lambda_{\max} = 340$ at STP. The concentration of the saturated solution was calculated from A_1 and A_2 employing Beer–Lambert's law, which yielded a K_{sp} value of 0.064 g L^{-1}.

Synthetic procedures

General information. All the reactions and sample preparations were carried out using standard Schlenk-line techniques or a glovebox in an inert argon environment unless stated. Freeze–pump–thaw cycles were utilized to degas commercially available methanol and triethylamine.

$[\{(MeOH)(\kappa^5\text{-L})\ Y\}_2(\mu_2, \kappa^2, \kappa^2\text{-}CO_3)]$, (2·Y). A 50 mL Schlenk flask was equipped with a magnetic stirring bar to which a solution of 0.1 mmol of lanthanide salt (64 mg of $Y(OTf)_3 \cdot 6H_2O$) in 5 ml of methanol was added to a slurry of

0.1 mmol of the ligand (40 mg of H_2L) in 5 ml of methanol. The mixture was stirred at room temperature for 30 minutes. The yellow precipitate was immediately visible after adding NEt_3 (0.30 mmol, 42 μL). After 15 min of stirring at room temperature, carbon dioxide gas was purged into the reaction mixture until the solution turned clear yellow. The reaction mixture was filtered and then concentrated under reduced pressure which gave bright yellow needle-shaped single crystals suitable for X-ray diffraction.

Isolated yield 55% (64 mg). UV-Vis: λ_{max} = 392 nm; $\varepsilon = 2.0 \times 10^4$ L mol^{-1} cm^{-1}; λ_{max} = 340 nm; $\varepsilon = 5.42 \times 10^4$ L mol^{-1} cm^{-1}; λ_{max} = 250 nm; $\varepsilon = 2.26 \times 10^4$ L mol^{-1} cm^{-1}; λ_{max} = 203 nm; $\varepsilon = 6.7 \times 10^4$ L mol^{-1} cm^{-1}. NMR (CD_3OD): δ ppm: ^{1}H: 2.64 (s, 12H, $-CH_3$), 7.40–7.50 (m, 16H, Aromatic-CH), 8.2–8.3 (m, 10H, aromatic –CH). IR (cm^{-1}): $\nu_{C=O}$ = 1552 (s); $\nu_{C=N}$ = 1640(w), 1586(m). Elemental analysis (%) calcd $C_{51}H_{54}N_{10}O_{11}Y_2$ (FW = 1160.86 g mol^{-1}): C 52.77; H 4.69; N 12.07; found: C 52.80; H 4.74; N 12.05.

[(κ^5-L) Y(κ^5-HL)], (4·Y). 0.1 mmol $Y(OTf)_3\cdot6H_2O$ (65 mg) and 0.2 mmol of the H_2L ligand (80 mg) along with 15 ml of methanol were mixed in a 50 mL single neck round-bottom flask equipped with a magnetic stirring bar. The reaction mixture was stirred at room temperature for 30 minutes, followed by the addition of 0.3 mmol of NEt_3 (42 μL). After 1 hour of stirring at room temperature, the reaction mixture was filtered and then concentrated under reduced pressure which gave block-shaped single crystals suitable for X-ray diffraction. The whole reaction was done under ambient conditions.

Isolated yield 70% (62 mg). UV-Vis: λ_{max} = 392 nm; $\varepsilon = 1.13 \times 10^4$ L mol^{-1} cm^{-1}; λ_{max} = 315 nm; $\varepsilon = 4.28 \times 10^4$ L mol^{-1} cm^{-1}; λ_{max} = 202 nm; and $\varepsilon = 6.27 \times 10^4$ L mol^{-1} cm^{-1}. NMR (CD_3OD): δ ppm: ^{1}H: 2.40 (s, 12H, $-CH_3$), 7.18–7.25 (m, 7H, aromatic-CH), 7.35–7.45 (m, 13H, aromatic-CH), 7.94–8.0 (d, 4H, aromatic –CH), 8.2–8.26 (t, 2H, aromatic –CH). IR (cm^{-1}): $\nu_{C=O}$ = 1558 (m); $\nu_{C=N}$ = 1644(w), 1582(m). Elemental analysis (%) calcd $C_{46}H_{39}N_{10}O_4Y$ (FW = 884.78 g mol^{-1}): C 62.44; H 4.44; N 15.83; found: C 62.48; H 4.46; N 15.80.

[(MeOH)(κ^5-L)Y(μ_2, κ^2, κ^2-CO_3)Y(κ^5-L)(Ph_3PO)], (5·Y). A 50 mL Schlenk flask was equipped with a magnetic stirring bar to which a solution of 0.1 mmol of lanthanide salt (64 mg of $Y(OTf)_3\cdot6H_2O$) in 5 ml of methanol was added to a slurry of 0.1 mmol of the ligand (40 mg of H_2L) in 5 ml of aqueous methanol and the mixture was stirred at room temperature for 30 minutes. The yellow precipitate was immediately visible after adding NEt_3 (0.30 mmol, 42 μL). After 15 min of stirring at room temperature, carbon dioxide gas was purged into the reaction mixture until the solution turned clear yellow, and after another 15 min, 0.1 mmol of TPPO was added and the reaction mixture was stirred for 6 hours. The reaction mixture was filtered and then concentrated under reduced pressure which gave yellow plate-shaped single crystals suitable for X-ray diffraction.

Isolated yield 40% (53 mg). UV-Vis: λ_{max} = 392 nm; $\varepsilon = 1.1 \times 10^4$ L mol^{-1} cm^{-1}; λ_{max} = 342 nm; $\varepsilon = 2.80 \times 10^4$ L mol^{-1} cm^{-1}; λ_{max} = 249 nm; $\varepsilon = 1.27 \times 10^4$ L mol^{-1} cm^{-1}; λ_{max} = 203 nm; and $\varepsilon = 5.74 \times 10^4$ L mol^{-1} cm^{-1}. NMR (CD_3OD): δ ppm: ^{1}H: 2.58 (s, 12H, $-CH_3$), 7.37–7.70 (m, 33H, aromatic-CH), 8.15–8.25 (m, 8H, aromatic –CH). 31P: 32.47. IR (cm^{-1}): $\nu_{C=O}$ = 1542 (m); $\nu_{C=N}$ = 1670(w), 1586(m). Elemental analysis (%) calcd $C_{66}H_{57}N_{10}O_9PY_2$ (FW = 1343.00 g mol^{-1}): C 59.03; H 4.28; N 10.43; found: C 59.06; H 4.32; N 10.40.

[{(MeOH)(κ^5-L) Er}$_2$(μ_2, κ^2, κ^2-CO_3)], (2·Er). A 50 mL Schlenk flask was equipped with a magnetic stirring bar to which a solution of 0.1 mmol of lanthanide salt (72 mg of $Er(OTf)_3\cdot6H_2O$) in 5 ml of methanol was added to a slurry of 0.1 mmol of the ligand (40 mg of H_2L) in 5 ml of methanol and the mixture was stirred at room temperature for 30 minutes. The yellow precipitate was immediately visible after adding NEt_3 (0.30 mmol, 42 μL). After 15 min of stirring at room temperature, carbon dioxide gas was purged into the reaction mixture until the solution turned clear yellow. The reaction mixture was filtered and then concentrated under reduced pressure which gave bright yellow needle-shaped single crystals suitable for X-ray diffraction.

Isolated yield 50% (64 mg). UV-Vis: λ_{max} = 392 nm; $\varepsilon = 2.1 \times 10^4$ L mol^{-1} cm^{-1}; λ_{max} = 341 nm; $\varepsilon = 5.80 \times 10^4$ L mol^{-1} cm^{-1}; λ_{max} = 249 nm; $\varepsilon = 2.60 \times 10^4$ L mol^{-1} cm^{-1}; λ_{max} = 203 nm; and $\varepsilon = 7.23 \times 10^4$ L mol^{-1} cm^{-1}. IR (cm^{-1}): $\nu_{C=O}$ = 1554 (s); $\nu_{C=N}$ = 1634(w), 1586(m). Elemental analysis (%) calcd $C_{51}H_{54}Er_2N_{10}O_{11}$ (FW = 1317.56 g mol^{-1}): C 46.49; H 4.13; N 10.63; found: C 46.55; H 4.10; N 10.60.

[(MeOH)(κ^5-L)Er(μ_2, κ^2, κ^2-CO_3)Er(κ^5-L)(Ph_3PO)], (5·Er). A 50 mL Schlenk flask was equipped with a magnetic stirring bar to which a solution of 0.1 mmol of lanthanide salt (72 mg of $Er(OTf)_3\cdot6H_2O$) in 5 ml of methanol was added to a slurry of 0.1 mmol of the ligand (40 mg of H_2L) in 5 ml of aqueous methanol and the mixture was stirred at room temperature for 30 minutes. The yellow precipitate was immediately visible after adding NEt_3 (0.30 mmol, 42 μL). After 15 min of stirring at room temperature, carbon dioxide gas was purged into the reaction mixture until the solution turned clear yellow, and after another 15 min, 0.1 mmol of TPPO was added and the reaction mixture was stirred for 6 hours. The reaction mixture was filtered and then concentrated under reduced pressure which gave yellow plate-shaped single crystals suitable for X-ray diffraction.

Isolated yield 42% (53 mg). UV-Vis: λ_{max} = 392 nm; $\varepsilon = 1.12 \times 10^4$ L mol^{-1} cm^{-1}; λ_{max} = 342 nm; $\varepsilon = 3.16 \times 10^4$ L mol^{-1} cm^{-1}; λ_{max} = 250 nm; $\varepsilon = 1.38 \times 10^4$ L mol^{-1} cm^{-1}; λ_{max} = 202 nm; and $\varepsilon = 6.13 \times 10^4$ L mol^{-1} cm^{-1}. IR (cm^{-1}): $\nu_{C=O}$ = 1540 (m); $\nu_{C=N}$ = 1670(w), 1586(m). Elemental analysis (%) calcd $C_{66}H_{57}Er_2N_{10}O_9P$ (FW = 1449.70 g mol^{-1}): C 52.86; H 3.83; N 9.34; found: C 52.90; H 3.86; N 9.36.

[(MeOH)(κ^5-L) Y(μ_2, κ^2, κ^2-CO_3)Y(κ^5-HL)(MeOH)](OTf), (1·Y), and [(MeOH)(κ^5-L)Y(μ_2, κ^2, κ^2-CO_3)Y(κ^5-L)(H_2O)], (3·Y). Neither **1·Y** nor **3·Y** was isolated in bulk in the pure phase. A 50 mL Schlenk flask was equipped with a magnetic stirring bar to which a solution of 0.1 mmol of lanthanide salt (64 mg of $Y(OTf)_3\cdot6H_2O$) in 5 ml of methanol was added to a slurry of 0.1 mmol of the ligand (40 mg of H_2L) in 5 ml of methanol and the mixture was stirred at room temperature for

30 minutes followed by the addition of NEt_3 (0.20 mmol, 28 μL). After 15 min of stirring at room temperature, carbon dioxide gas was purged into the dark yellow reaction mixture until the solution turned light yellow. The reaction mixture was filtered and then concentrated under reduced pressure which yielded a physical mixture of single crystals of **1·Y**, **2·Y** and **3·Y**.

[{(Ph_3PO)(κ^5-L) Y}$_2$(μ_2, κ^2, κ^2-CO_3)], (6·Y). The complex, **6·Y**, was not isolated in bulk in the pure phase. A 50 mL Schlenk flask was equipped with a magnetic stirring bar to which a solution of 0.1 mmol of lanthanide salt (64 mg of $Y(OTf)_3\cdot 6H_2O$) in 5 ml of methanol was added to a slurry of 0.1 mmol of the ligand (40 mg of H_2L) in 5 ml of aqueous methanol and the mixture was stirred at room temperature for 30 minutes. The yellow precipitate was immediately visible after adding NEt_3 (0.30 mmol, 42 μL). After 15 min of stirring at room temperature, carbon dioxide gas was purged into the reaction mixture until the solution turned clear yellow, and after another 15 min, 0.2 mmol of TPPO was added and the reaction mixture was stirred for 6 hours. The reaction mixture was filtered and then concentrated under reduced pressure which resulted in a physical mixture of single crystals of **5·Y** and **6·Y**.

Results and discussion

Synthesis and spectroscopic characterization

The *as-synthesized* solid sample of H_2L appears off-white in color and it is sparingly soluble in methanol at STP. A white slurry of H_2L in commercially available methanol (with ~1%, v/v, water content) turned immediately into bright, golden yellow solution with concomitant consumption of the white suspended particles of H_2L upon the addition of a methanolic solution of Y(III) salt – implying complexation of the ligand with the metal ions (Scheme 1). The reaction solution displayed two distinct sets of signals in its ^1H NMR spectrum (δ (CH_3, ppm) = 2.83 and 2.71; Fig. 1). The ^1H NMR spectral behavior could be attributed to the probable products as depicted in Scheme S1 (see the ESI†). As per our previous experience, H_2L can afford double deprotonation.[8] Therefore, the reaction mixtures were charged with two equivalents of Et_3N as a base. The reaction solution appeared dark yellow immediately upon addition of Et_3N, indicating deprotonation of the ligand.[8] The ^1H NMR spectrum of the resulting solution revealed two new sets of signals (δ (CH_3, ppm) = 2.72 and 2.40; Fig. 1). Fortunately, the mononuclear decacoordinate complex, **4·Y**, crystallized out of the reaction mixture ((a) followed by (b), Scheme 1). The ^1H NMR spectroscopic analyses on the isolated sample of **4·Y** revealed that the signal appearing at δ = 2.40 ppm corresponds to the CH_3 protons of **4·Y** (Fig. S3, see the ESI†).

The purging of CO_2 gas into the reaction mixtures changed the dark-yellow solutions into light-yellow solutions. The ^1H NMR spectrum of the reaction mixture ((a) followed by (b) followed by (c), Scheme 1) implied dominantly one product other than **4·Y** (Fig. 1). Visibly slightly different types of single crystals were found to appear from the reaction solutions upon concentrating the reaction mixtures under reduced pressure. The crystallographically characterized complexes include **1·Y–4·Y**, as depicted in Scheme 1. Notably, **1·Y** and **3·Y** were found to deteriorate spontaneously at room temperature upon isolation from their mother liquors. Though the molecular structures of **1·Y** and **3·Y** were unambiguously characterized by single crystal X-ray diffraction analyses, we could not purify them in bulk. However, the chemical shift at 2.72 ppm in the ^1H NMR spectrum could be attributed to the CH_3 moieties of the ligand in **1·Y** (Fig. 1).

Characterization of the cationic dinuclear analogue (**1·Y**) prompted us to repeat the same reactions but employing three equivalents of Et_3N instead of two equivalents of Et_3N. In order for generality, both Y(III) and Er(III) salts were employed in the reactions. The observations were found to be similar for both of them. However, the reaction mixtures ((a) followed by (d); Scheme 1) resulted in a fluorescent, gelatinous yellow precipitate immediately upon addition of three equivalents of Et_3N under the same conditions. The whole reaction mixture turned into a translucent yellow solution immediately upon purging CO_2 gas into the reaction mixture under stirring conditions at STP. The ^1H NMR spectrum of the reaction mixture ((a) followed by (d) followed by (c)) of the Y analogue revealed the presence of only the neutral dinuclear complex (**2·Ln**, Fig. 1) where both the terminally axial coordination sites are occupied by MeOH. The mononuclear decacoordinate complex (**4·Ln**) was also detected as the minor product which was carried forward from the previous steps of the reactions. However, purging of CO_2 gas was discontinued once the yellow precipitate was visibly consumed completely. Bright yellow, plate-shaped single crystals of **2·Ln** (Ln = Y and Er) started to crash out of the reaction solutions within a few minutes depending on the concentration of the reaction solutions. Notably, the outcome of the reaction was found to be independent of the amount of the employed Et_3N once it exceeded three equivalents.

In order to investigate the efficiency of the capture and conversion of CO_2 gas, the gas-phase FT-IR spectroscopic studies in conjunction with the gasometer spectroscopic analyses were carried out on the headspace of the reaction mixtures (see the Experimental section for details). No trace of CO_2 was detected in the headspace within 20 minutes of the reaction time (Fig. 2). Considering a very low solubility product of CO_2 in aqueous methanol,[12] the above observation can be regarded as the quantitative consumption of the employed CO_2 gas. It is worth pointing out that the dinuclear complexes, **2·Ln**, can also be achieved with excellent yields upon performing the reactions (a) followed by (d) (Scheme 1) under open atmospheric conditions without employing any CO_2 gas as a reagent. The bridging CO_3^{2-} in the complexes originated from the open atmosphere despite the partial pressure of CO_2 gas under an open atmosphere being very low (<0.25 mmHg), implying the high efficiency of capturing CO_2 and converting it into CO_3^{2-}.

The dinuclear carbonato-bridged complexes **2·Ln** are air-stable both in solution and in the solid state indefinitely.

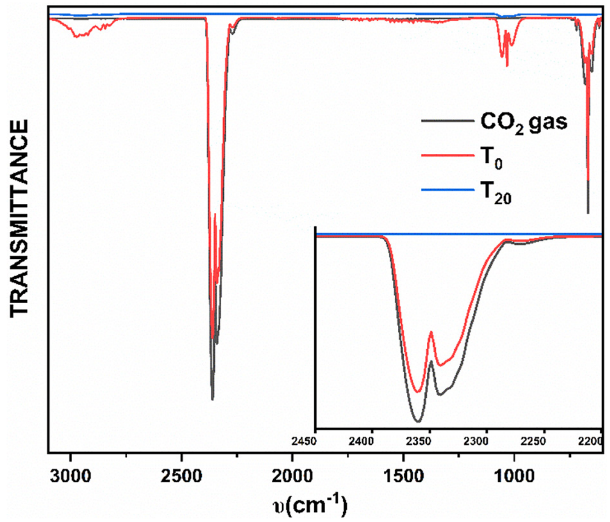

Fig. 2 The comparative gas-phase IR spectra of free CO_2 gas (black), headspace of the reaction mixture in the beginning (T_0, red) and headspace of the reaction mixture after 20 minutes (T_{20}, blue).

Thus, we intended to investigate if the coordinated MeOH in **2·Ln** could be deliberately replaced with stronger Lewis bases. In this regard, **2·Ln** were treated with Ph_3PO. The progress of the reactions was monitored by multinuclear (^1H and ^{31}P) NMR spectroscopic studies on the reaction mixtures of the Y analogues. Indeed, treatment of **2·Ln** with one equivalent of Ph_3PO rendered substitution of the coordinated MeOH with Ph_3PO at one of the terminally axial coordination sites, resulting in **5·Ln** (Ln = Y and Er) with near-quantitative yields. Notably, the conversion of **2·Ln** into **6·Ln** was found to be low-yielding even upon employment of excess Ph_3PO. It can be ascribed to the following reasons. **2·Ln** is sparingly soluble (~10^{-5} mol L^{-1}) in MeOH at STP. Consequently, the substitution reactions were carried out under significantly dilute conditions. As MeOH is present in the reaction mixture at an enormously large excess compared to Ph_3PO, the formation of **5·Ln** is kinetically more favorable over the formation of **6·Ln** according to Le Chatelier's principle. Moreover, the solubility products of both **5·Ln** and **6·Ln** are quite similar to each other in MeOH. **6·Y** can be isolated in pure form with a very low yield by manual separation of its single crystals from the physical mixture of the single crystals of **5·Y** and **6·Y**. The ^1H NMR spectral analysis of **6·Y** reveals that it slowly transforms into **5·Y** in solution (Fig. S7, see the ESI†). On the other hand, **5·Y** is found not to equilibrate with **6·Y** even upon prolonged standing in methanolic solution. Sharp and considerably downfield shifted ^{31}P NMR signals for **5·Y** (32.47 ppm) and **6·Y** (32.55 ppm) compared to the free Ph_3PO (32.39 ppm) indicated considerably stronger coordination of Ph_3PO to the Ln centers (Fig. S10, see the ESI†). ^1H NMR spectroscopic analyses also indicated stronger coordination of Ph_3PO to the Ln centers (Fig. 1 and S6–S8, see the ESI†). Unfortunately, we could not isolate and characterize the Er analogue of **6·Ln** despite various efforts.

The FT-IR spectral profiles of the isolated complexes appear similar to each other, implying a similar degree of metal–ligand chelation (Fig. S13, S14 and Tables S3, S4, see the ESI†). Notably, the yellow coloration of the Ln(III) complexes with the doubly deprotonated forms of the analogous Schiff base ligands is known to originate from the ligand-to-metal charge transfer.[8] All of **2·Ln**, **4·Ln** and **5·Ln** exhibit absorption bands in four different domains of the UV-vis range (Fig. S11, S12 and Tables S1, S2, see the ESI†). The spectral patterns of the series **4·Ln** are distinctly different from those of **2·Ln** and **5·Ln**. Though the spectral patterns of **2·Ln** and **5·Ln** are practically indistinguishable from each other, their molar extinction coefficients were found to be significantly different from each other.

X-ray crystallographic characterization

Both the Y and Er analogues for a given series of the complexes are isostructural. Therefore, the crystallographic characteristics of the Y analogues are presented in the main text as the representatives for their respective series. Notably, the Er(III) analogue of the mononuclear decacoordinate complex, **4·Er**, has already been reported.[13] The solid-state single crystal X-ray molecular structures for **1·Y**, **2·Y**, **3·Y**, **5·Y** and **6·Y** are portrayed in Fig. 3. The solid-state single-crystal molecular structures of the rest of the complexes and the associated crystallographic parameters are provided in the ESI (Fig. S15–S30 and Tables S5, S6†). The molecular skeletons of all the dinuclear complexes are mutually similar to each other as follows. A pentadentate ligand chelates an Ln ion in the κ^5-fashion by coordinating through its pyridyl N atom, two imine N atoms and two carbonyl O atoms, resulting in a pseudo pentagonal building block (Fig. 3). Except for **1·Y** and **4·Y**, the pentadentate chelating ligand was found to be doubly deprotonated, which could be concluded from the following observations. The statistical single crystal X-ray diffraction analyses on the coordination complexes of the analogous Schiff base ligands revealed that the crystallographic bond angles associated with the hydrazide functional groups (*ca.* <C17–N1–N2 in **1·Y**, Table S7, see the ESI†) fall below a threshold value of 111° if the amide N center is deprotonated,[8,14] while they fall above the threshold value when the amide N center remains protonated. In the case of the cationic dinuclear complex herein (**1·Y**), one of such angles (<C17–N1–N2 = 112.42°) falls above the threshold values, while the rest of such angles fall below the threshold values (108.81°–110.35°, Table S7, see the ESI†).

Similarly, for the mononuclear decacoordinate complexes (**4·Y**), out of the two pentadentate chelating ligands, one is doubly deprotonated, while the other one is singly deprotonated. The bond parameters of the bridging CO_3 moieties imply a doubly negative charge in it. Thus, the overall charges on the complexes also indicate the same conclusion.

Photoluminescence property studies

Because of the characteristic electronic structures, the lanthanide ions are expected to possess immense potential in tuning and tailoring varieties of photophysical phenomena, especially

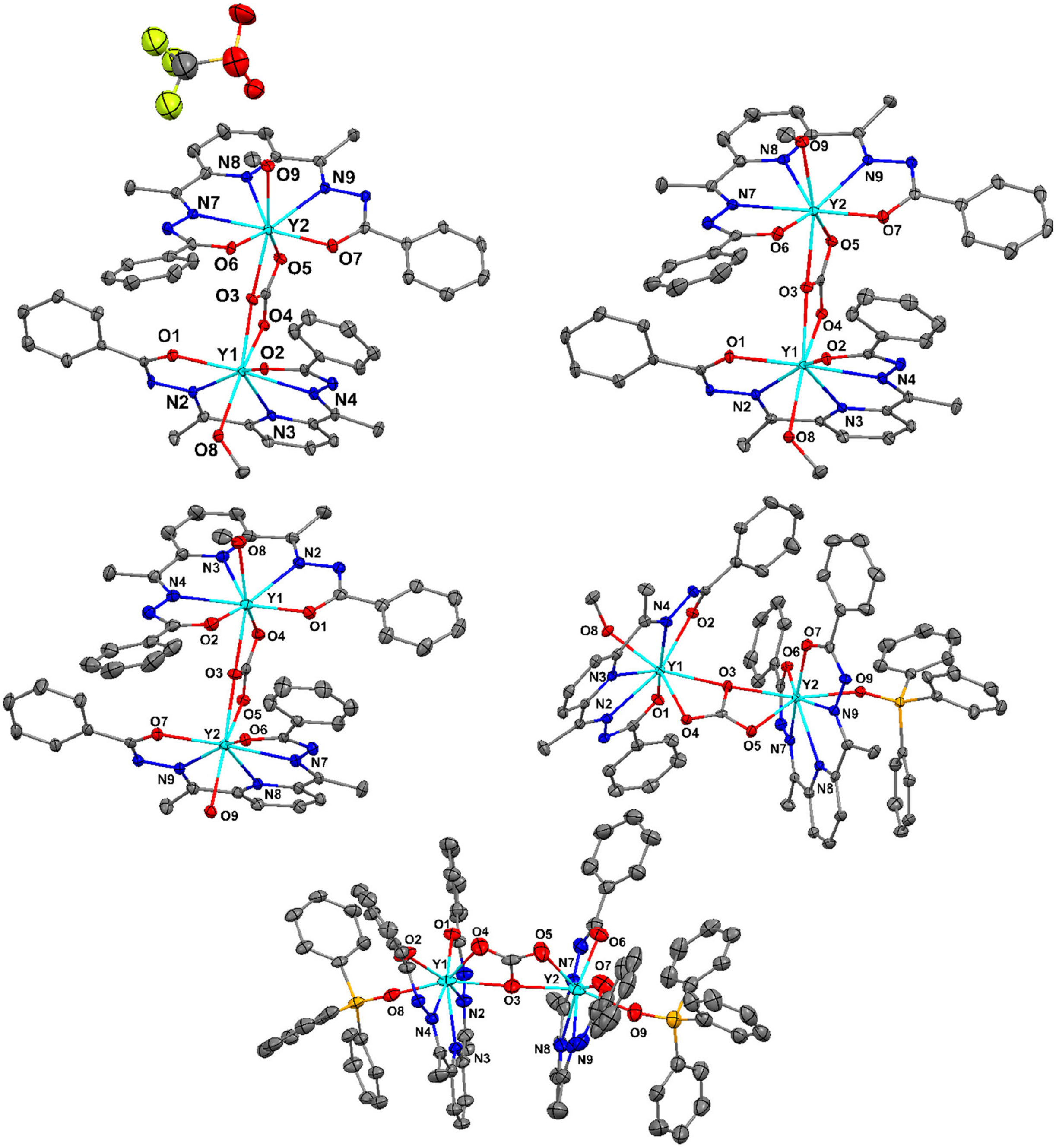

Fig. 3 ORTEP representations with 40% ellipsoid probability for the solid-state single crystal X-ray molecular structures of **1·Y** (top left), **2·Y** (top right), **3·Y** (middle left), **5·Y** (middle right), and **6·Y** (bottom). The atomic sites of the inner coordination environments are labelled. The H atoms and the co-crystallized solvent molecules are omitted for clarity. Color codes: cyan, Y; yellow, S; orange, P; greenish yellow, F; red, O; blue, N; and grey, C.

photoluminescence (PL).[15] However, the valence orbitals (4f) are in the inner cores of the lanthanide ions.[4b] Thus, the influence of the ligand field on the energy landscapes of the spectroscopic terms is not prominent.[15b] Consequently, modulating spectroscopic characteristics that originated from the lanthanide ions is challenging.[15e] Moreover, the spectroscopic characteristics are subject to the coordination geometry and ligand-field topology around the metal ions. On the other hand, the lanthanide coordinative bonds are significantly ionic in nature. Thus, it is non-trivial to rigidify a specific coordination geometry around the lanthanide ions and to tailor the spectroscopic properties.[15b] However, the continuous SHAPE analyses[16] revealed fairly rigid coordination geometries around the metal ions of the dinuclear lanthanide motifs described herein (Table S8, see the ESI†). In addition to it, the terminally axial coordination sites are kinetically labile. The

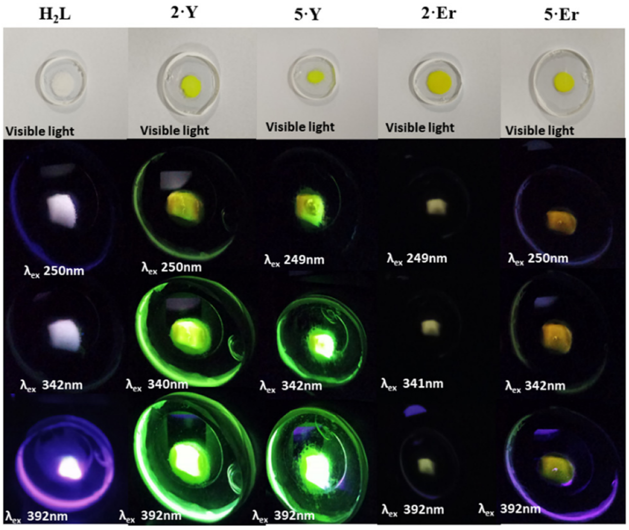

Fig. 4 The appearances of the *as-synthesized* solid samples of H_2L (first column), **2·Y** (second column), **5·Y** (third column), **2·Er** (fourth column) and **5·Er** (fifth column) upon irradiation with different wavelengths at room temperature (see the experimental section for details).

electronic and crystal-field effects of the dinuclear complexes could be tailored by tuning various ancillary ligands at the terminally axial coordination sites. Moreover, these dinuclear motifs could be chemically decorated with a huge variety of Schiff-base ligands of the genre H_2L. In this regard, we intended to investigate the detailed PL properties both in solutions and in the solid states of dinuclear complexes **2·Ln** and **5·Ln** (Ln = Y and Er) which were isolated in bulk with phase purity (see the Experimental section for details).

The *as-synthesized* solid sample of H_2L appeared off-white under visible light at room temperature (Fig. 4). It appeared brighter upon irradiation with the UV-vis light. Both **2·Y** and **5·Y** appeared bright yellow under visible light at room temperature, which turned into glowing green under irradiation with UV-vis light (Fig. 4). Notably, the Er analogues were found to be not as bright as their Y analogues under irradiation with similar light (Fig. 4). However, the brightest appearance was found to be upon excitation near 390 nm for all of H_2L, **2·Ln** and **5·Ln** (Fig. 4). The room temperature PL excitation spectral analyses of the *as-synthesized* samples of H_2L, **2·Ln** and **5·Ln** (Ln = Y and Er) revealed characteristic emission bands

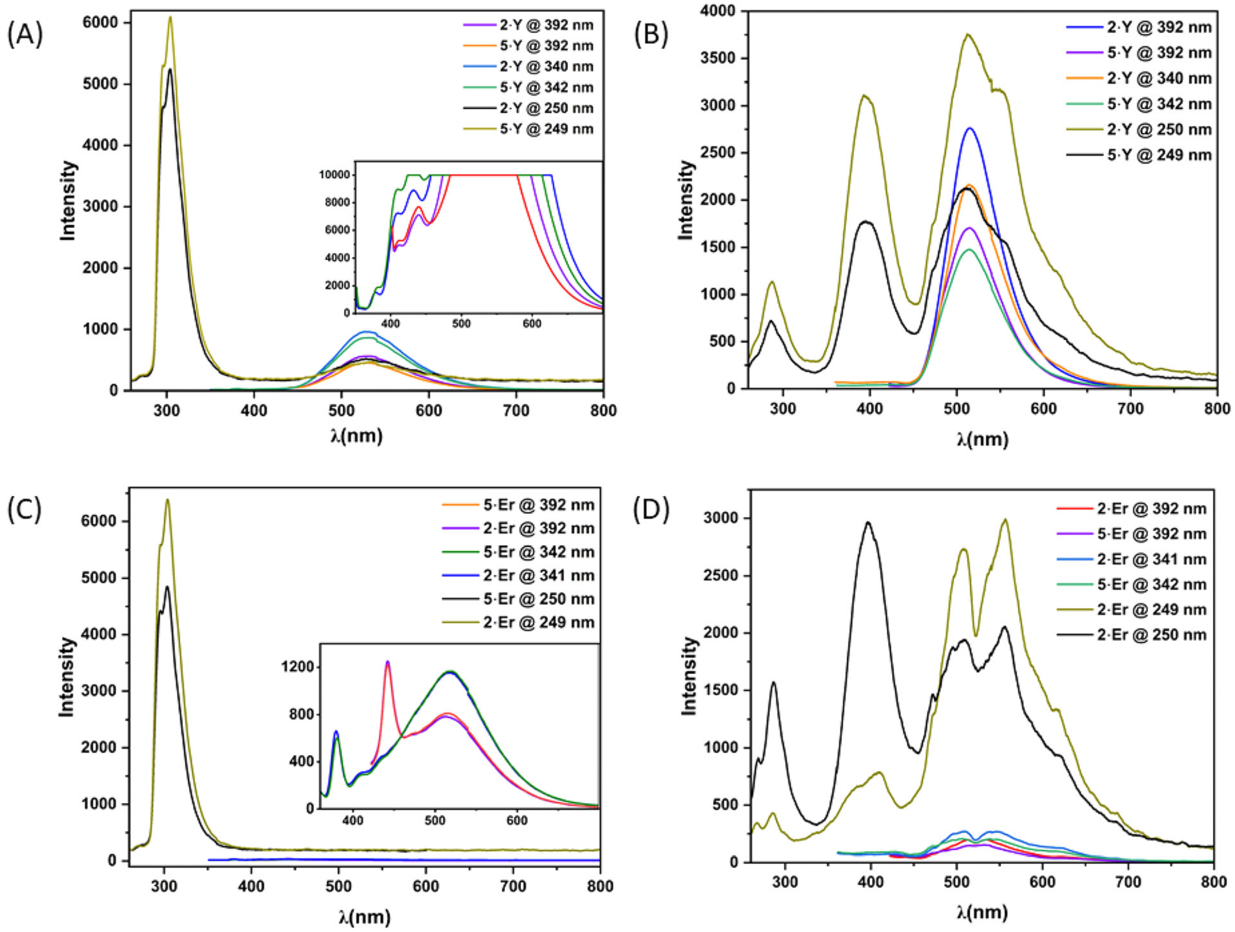

Fig. 5 The photoluminescence (PL) spectra of the *as-synthesized* samples of **2·Ln** and **5·Ln** (Ln = Y and Er) in methanolic solutions ((A) for Y and (C) for Er analogues) and in solid states ((B) for Y and (D) for Er analogues). All the spectra in the figures were recorded at room temperature with slit-widths of 2.5 nm for both excitation and emission. The spectra in the insets were recorded at room temperature with slit-widths of 10 nm for excitation and 5 nm for emission.

(Fig. S33–S39†). H_2L exhibited structured emission spectra having significantly overlapping emission bands with emission maxima near 625 nm, 550 nm, 475 nm, 450 nm and 425 nm (Fig. S33, see the ESI†). Both **2·Ln** and **5·Ln** exhibited strong emission bands near the emission maximum of 310 nm upon excitation near 250 nm in their methanolic solutions at room temperature (Fig. 5). Though the Y analogues displayed prominently broad bands near the emission maximum of 540 nm consistently for all the excitations near 390 nm, 340 nm and 250 nm, no emission band was observed above the emission wavelength of 350 nm for the Er analogues under the same conditions (Fig. 5). The room temperature solid-state emission spectral profiles for both **2·Ln** and **5·Ln** were found to be similar to each other upon excitation near 250 nm, displaying bands near the emission maxima of 300 nm, 400 nm, 500 nm and 550 nm (Fig. 5). The strongest emission bands were observed near the emission maxima of 550 nm for **2·Er**, 520 nm for **2·Y** and **5·Y**, and 400 nm for **5·Er**. Notably, the solid samples of **2·Y** and **5·Y** exhibited bands near the emission maximum of 520 nm with significantly high emission intensities upon excitations near 340 nm and 390 nm, where the Er analogues displayed very weak emission bands. It is in line with the observation that the solid samples of Y analogues appeared way brighter than their Er analogues under the irradiation with the UV-vis light. It is worth mentioning that all the above PL spectral studies were carried out with the slit widths of 2.5 nm for both excitation ($\Delta l_{\text{ex.}}$) and emission ($\Delta l_{\text{em.}}$). The room temperature emission spectra of the methanolic solutions of the Er analogues revealed prominent bands near the emission maximum of 520 nm for the excitations near 390 nm and 340 nm upon increasing the slit widths (insets, Fig. 5). In addition to the emission bands with the emission maxima near 520 nm, the spectra also displayed relatively sharp, prominent bands near emission maxima of 380 nm and 450. However, the Y analogues exhibited enormously high emission intensity in the same spectral range in the same experimental set-up (inset, Fig. 5). It could be attributed to the following reason. All the emission bands herein are characteristic of the ligand. The electronic transitions characteristic of the spectroscopic terms of the Er(III) ion also span over the lower energy spectral range herein.[15,17] Upon excitation of the Er analogues, it could lead to the spin–phonon coupling and subsequent non-radiative spin–lattice/Orbach relaxation at room temperature, thereby quenching the emission for the Er analogues.[18]

Mechanistic aspects

The widely accepted mechanism for the fixation of CO_2 into CO_3^{2-} is as follows: dissolution of CO_2 gas followed by carbonation of water to produce carbonic acid and subsequent ionization of carbonic acid into bicarbonate/carbonate before complexation with metal ions.[3g,5f] For a carbonato Ln complex with the usual bridging mode(s) of CO_3^{2-}, the aforementioned mechanism might be operative. However, there is also precedence for the formation of Ln-based carbonato complexes in non-polar solvents under anhydrous conditions.[5i] Moreover, the formation of cluster complexes with extremely short non-covalent distances between the coordinated carbonates is also evidenced.[5g] Therefore, the existence of additional alternative pathway(s) for the fixation of CO_2 into carbonato complexes could probably not be ruled out.

Conclusions

In conclusion, Ln ions in conjunction with the Schiff base ligands of the genre H_2L possess immense potential for facile fixation of CO_2 under ambient conditions. The carbonato-bridged dinuclear Ln(III) cores are equipped with the kinetically labile terminally axial coordination sites of the Ln centers, which could afford inner coordination post-synthetic modifications. The feasibility for the post-synthetic modification opens up an opportunity to tailor hierarchical physicochemical properties by employing various ancillary ligands. The dinuclear complexes were also found to be UV-vis active with strong molar extinction coefficients at room temperature. They also exhibited photoluminescence both in solid state and in solution with significantly large emission intensities at room temperature. The photophysical properties of the dinuclear complexes were found to be significantly different from those of the pristine ligand. Moreover, both the UV-vis and PL spectral characteristics were found to be considerably susceptible to the ancillary ligands at the terminally axial coordination sites of the dinuclear motifs.

Author contributions

The manuscript was written through contributions from all the authors. All the authors have given approval to the final version of the manuscript.

Data availability

All the data related to the article are provided in the ESI.† Crystallographic data are also deposited in the form of CIF files at the Cambridge Crystallographic Data Centre with reference number CCDC 2378627–2378634.† Any additional associated experimental details and relevant data can be obtained from the authors upon request.

Conflicts of interest

There are no conflicts to declare.

Acknowledgements

AKB thanks the Empowerment and Equity Opportunities for Excellence in Science (EEQ/2021/000800), and the Science and

Engineering Research Board (SERB), for the financial support to carry out the research.

References

1 H. Ritchie, P. Rosado and M. Roser, "Our World in Data: CO_2 and Greenhouse Gas Emissions", https://ourworldindata.org/co2-and-greenhouse-gas-emissions, 2022.

2 P. Gabrielli, M. Gazzani and M. Mazzotti, *Ind. Eng. Chem. Res.*, 2020, **59**, 7033–7045.

3 (*a*) C. Xia, P. Zhu, Q. Jiang, Y. Pan, W. Liang, E. Stavitski, H. N. Alshareef and H. Wang, *Nat. Energy*, 2019, **4**, 776–785; (*b*) V. Kumaravel, J. Bartlett and S. C. Pillai, *ACS Energy Lett.*, 2020, **5**, 486–519; (*c*) K. Sumida, D. L. Rogow, J. A. Mason, T. M. McDonald, E. D. Bloch, Z. R. Herm, T.-H. Bae and J. R. Long, *Chem. Rev.*, 2012, **112**, 724–781; (*d*) M. Ding, R. W. Flaig, H.-L. Jiang and O. M. Yaghi, *Chem. Soc. Rev.*, 2019, **48**, 2783–2828; (*e*) H. Demir, G. O. Aksu, H. C. Gulbalkan and S. Keskin, *Carbon Capture Sci. Technol.*, 2022, **2**, 100026–100038; (*f*) D. A. Palmer and R. van Eldik, *Chem. Rev.*, 1983, **83**, 651–731; (*g*) K. Sołtys-Brzostek, M. Terlecki, K. Sokołowski and J. Lewiński, *Coord. Chem. Rev.*, 2017, **334**, 199–231; (*h*) J. Wu, X.-L. Li, L. Zhao, M. Guo and J. Tang, *Inorg. Chem.*, 2017, **56**(7), 4104–4111.

4 (*a*) R. G. Pearson, *J. Am. Chem. Soc.*, 1963, **85**, 3533–3539; (*b*) R. A. Layfield and M. Murugesu, *Lanthanides and Actinides in Molecular Magnetism*, Wiley VCH, 2015.

5 (*a*) K. Griffiths, J. Mayans, M. A. Shipman, G. J. Tizzard, S. J. Coles, B. A. Blight, A. Escuer and G. E. Kostakis, *Cryst. Growth Des.*, 2017, **17**, 1524–1538; (*b*) K. Ehama, Y. Ohmichi, S. Sakamoto, T. Fujinami, N. Matsumoto, N. Mochida, T. Ishida, Y. Sunatsuki, M. Tsuchimoto and N. Re, *Inorg. Chem.*, 2013, **52**, 12828–12841; (*c*) S. Sakamoto, T. Fujinami, K. Nishi, N. Matsumoto, N. Mochida, T. Ishida, Y. Sunatsuki and N. Re, *Inorg. Chem.*, 2013, **52**, 7218–7229; (*d*) S. Sakamoto, S. Yamauchi, H. Hagiwara, N. Matsumoto, Y. Sunatsuki and N. Re, *Inorg. Chem. Commun.*, 2012, **26**, 20–23; (*e*) S. Titos-Padilla, J. Ruiz, J. M. Herrera, E. K. Brechin, W. Wersndorfer, F. Lloret and E. Colacio, *Inorg. Chem.*, 2013, **52**, 9620–9626; (*f*) N. Qiao, X.-Y. Xin, X.-F. Guan, C.-X. Zhang and W.-M. Wang, *Inorg. Chem.*, 2022, **61**, 15098–15107; (*g*) V. Velasco, D. Aguila, L. A. Barrios, I. Borilovic, O. Roubeau, J. Ribas-Arino, M. Fumanal, S. J. Teatd and G. Aromi, *Chem. Sci.*, 2015, **6**, 123–131; (*h*) T. D. Pasatoiu, A. Ghirri, A. M. Madalan, M. Affronte and M. Andruh, *Dalton Trans.*, 2014, **43**, 9136–9142; (*i*) S. Maity, A. Mondal, S. Konar and A. Ghosh, *Dalton Trans.*, 2019, **48**, 15170–15183; (*j*) A. R. Willauer, M. Laurent, D. Toniolo, F. Fadaei-Tirani, Y. Yang and M. Mazzanti, *Dalton Trans.*, 2019, **48**, 6100–6110; (*k*) H. Tian, L. Zhao and J. Tang, *Cryst. Growth Des.*, 2018, **18**, 1173–1181; (*l*) C. H. Hossack, R. J. Butcher, C. L. Cahill and C. Besson, *Inorg. Chem.*, 2021, **60**, 15724–15743; (*m*) H. Tian, M. Wang, L. Zhao, Y.-N. Guo, Y. Guo, J. Tang and Z. Liu, *Chem. – Eur. J.*, 2012, **18**, 442–445; (*n*) H.-R. Wen, J.-J. Hu, K. Yang, J.-L. Zhang, S.-J. Liu, J.-S. Liao and C.-M. Liu, *Inorg. Chem.*, 2020, **59**, 2811–2824; (*o*) C. Browne, W. J. Ramsay, T. K. Ronson, J. Medley-Hallam and J. R. Nitschke, *Angew. Chem., Int. Ed.*, 2015, **54**, 11122–11127; (*p*) L. Armelao, D. B. D. Amico, P. Biagini, G. Bottaro, S. Chiaberge, P. Falvo, L. Labella, F. Marchetti and S. Samaritani, *Inorg. Chem.*, 2014, **53**, 4861–4871; (*q*) S. K. Langley, B. Moubaraki and K. S. Murray, *Inorg. Chem.*, 2012, **51**, 3947–3949; (*r*) C.-M. Liu, D.-Q. Zhang, X. Hao and D.-B. Zhu, *Dalton Trans.*, 2020, **49**, 2121–2128; (*s*) T. N. Hooper, R. Inglis, M. A. Palacios, G. S. Nichol, M. B. Pitak, S. J. Coles, G. Lorusso, M. Evangelisti and E. K. Brechin, *Chem. Commun.*, 2014, **50**, 3498–3500; (*t*) W.-M. Wang, X.-Y. Xin, N. Qiao, Z.-L. Wu, L. Lib and J.-Y. Zou, *Dalton Trans.*, 2022, **51**, 13957–13969; (*u*) H. Tian, L. Zhao, Y.-N. Guo, Y. Guo, J. Tang and Z. Liu, *Chem. Commun.*, 2012, **48**, 708–710; (*v*) J. Vallejo, J. Cano, I. Castro, M. Julve, F. Lloret, O. Fabelo, L. Canadillas-Delgadoz and E. Pardo, *Chem. Commun.*, 2012, **48**, 7726–7728; (*w*) S. Xue, L. Zhao, Y.-N. Guo, P. Zhangab and J. Tang, *Chem. Commun.*, 2012, **48**, 8946–8948; (*x*) H. Ke, L. Zhao, G.-F. Xu, Y.-N. Guo, J. Tang, X.-Y. Zhang and H.-J. Zhang, *Dalton Trans.*, 2009, 10609–10613; (*y*) K. Ehama, Y. Ohmichi, S. Sakamoto, T. Fujinami, N. Matsumoto, N. Mochida, T. Ishida, Y. Sunatsuki, M. Tsuchimoto and N. Re, *Inorg. Chem.*, 2013, **52**, 12828–12841; (*z*) W. Sethi, S. Sanz, K. S. Pedersen, M. A. Sørensen, G. S. Nichol, G. Lorusso, M. Evangelisti, E. K. Brechin and S. Piligkos, *Dalton Trans.*, 2015, **44**, 10315–10320.

6 (*a*) F.-S. Guo, A. K. Bar and R. A. Layfield, *Chem. Rev.*, 2019, **119**, 8479; (*b*) A. K. Bar, P. Kalita, M. K. Singh, G. Rajaraman and V. Chandrasekhar, *Coord. Chem. Rev.*, 2018, **367**, 163.

7 S. Cotton, *Lanthanide and Actinide Chemistry*, John Wiley & Sons, Ltd, 2006.

8 (*a*) P. Kalita, N. Ahmed, S. Moorthy, V. Béreau, A. K. Bar, P. Kumar, P. Nayak, J.-P. Sutter, S. K. Singh and V. Chandrasekhar, *Dalton Trans.*, 2023, **52**, 2804–2815; (*b*) P. Kalita, N. Ahmed, A. K. Bar, S. Dey, A. Jana, G. Rajaraman, J.-P. Sutter and V. Chandrasekhar, *Inorg. Chem.*, 2020, **59**, 6603–6612; (*c*) A. K. Bar, P. Kalita, J.-P. Sutter and V. Chandrasekhar, *Inorg. Chem.*, 2018, **57**, 2398–2401; (*d*) V. Singh, D. Das, S. Anga, J.-P. Sutter, V. Chandrasekhar and A. K. Bar, *ACS Omega*, 2022, **7**, 25881–25890; (*e*) V. Singh, L. T. Suresh, J.-P. Sutter and A. K. Bar, *Dalton Trans.*, 2024, **53**, 7436–7449.

9 C. Lorenzini, C. Pelizzi, G. Pelizzi and G. Predieri, *J. Chem. Soc., Dalton Trans.*, 1983, **4**, 721–727.

10 L. Dubovan, A. Pollnitz and C. Silvestru, *Eur. J. Inorg. Chem.*, 2016, **10**, 1521–1527.

11 International Tables for Crystallography, DOI: 10.1107/97809553602060000001.

12 M. Décultot, A. Ledoux, M.-C. Fournier-Salaün and L. Estel, *J. Chem. Thermodyn.*, 2019, **138**, 67–77.

13 T. A. Bazhenova, I. A. Yakushev, K. A. Lyssenko, O. V. Maximova, V. S. Mironov, Y. V. Manakin, A. B. Kornev, A. N. Vasiliev and E. B. Yagubskii, *Magnetochemistry*, 2020, **6**, 60–86.

14 J.-P. Sutter, V. Béreau, V. Jubault, K. Bretosh, C. Pichon and C. Duhayon, *Chem. Soc. Rev.*, 2022, **51**, 3280–3313.

15 (*a*) A. de Bettencourt-Dias, *Inorg. Chem.*, 2016, **55**, 3199–3202; and the references therein; (*b*) A. de Bettencourt-Dias, Introduction to Lanthanide Ion Luminescence, in *Luminescence of Lanthanide Ions in Coordination Compounds and Nanomaterials*, ed. A. de Bettencourt-Dias, John Wiley & Sons, Ltd, Chichester, United Kingdom, 2014, pp. 1–48; (*c*) Y. Hasegawa, Y. Kitagaw and T. Nakanishi, *NPG Asia Mater.*, 2018, **10**, 52–70; (*d*) S. Lis, *J. Alloys Compd.*, 2002, **341**, 45–50; (*e*) R. C. Leif, L. M. Vallarino, M. C. Becker and S. Yang, *Cytometry, Part A*, 2006, **69A**, 767–778; (*f*) M. Hasegawa, H. Ohmagari, H. Tanaka and K. Machida, *J. Photochem. Photobiol., C*, 2022, **50**, 100484–100511; (*g*) I. Hemmila, *J. Alloys Compd.*, 1995, **225**, 480–485.

16 M. C. D. Llunell, J. Cirera, P. Alemany and S. Alvarez, *SHAPE program, version 2*, Universitat de Barcelona, Barcelona, Spain, 2010.

17 (*a*) W. T. Carnall, P. R. Fields and K. Rajnak, *J. Chem. Phys.*, 1968, **49**, 4424–4442; (*b*) M. Irfanullah and K. Iftikhar, *J. Fluoresc.*, 2011, **21**, 81–93.

18 (*a*) R. Orbach, *Proc. R. Soc. A*, 1968, **264**, 458–484; (*b*) G. H. Larson and C. D. Jeffries, *Phys. Rev.*, 1966, **141**, 461–478; (*c*) L. E. Nodaraki, A.-M. Ariciu, D. N. Huh, J. Liu, D. O. T. A. Martins, F. Ortu, R. E. P. Winpenny, N. F. Chilton, E. J. L. McInnes, D. P. Mills, W. J. Evans, F. Tuna and J. Am, *Chem. Soc.*, 2024, **146**(22), 15000–15009.